


Photon-assisted electron transport across a quantum phase transition

Lei-Lei Nian¹, Shiqian Hu¹, Long Xiong^{1,*}, Jing-Tao Lü^{2,†} and Bo Zheng^{1,3,‡}

¹*School of Physics and Astronomy, Yunnan University, Kunming 650091, Peoples Republic of China*

²*School of Physics, Institute for Quantum Science and Engineering, Wuhan National High Magnetic Field Center, Huazhong University of Science and Technology, Wuhan 430074, Peoples Republic of China*

³*Collaborative Innovation Center of Advanced Microstructures, Nanjing University, Nanjing 210093, Peoples Republic of China*

 (Received 28 June 2023; revised 7 August 2023; accepted 15 August 2023; published 28 August 2023)

Quantum-dot circuit quantum electrodynamics (QD-cQED) offers an important platform for achieving photon-to-electron conversion in the linear regime, but it has been challenging to efficiently control the photocurrent. Here, we propose a nonlinear QD-cQED setup of a double quantum dot system capacitively coupled to a microwave resonator containing Kerr nonlinearity. By means of the quantum master equation, we derive a general formulation to establish the connection between photon excitation and generated photocurrent. It is revealed that the excitation of photons undergoes a first-order quantum phase transition, which provides a mechanism to adjust the photon-assisted electron transport and leads to an increase in the photocurrent. In contrast to the linear QD-cQED setups, the enhancement in photocurrent benefits from the enhanced energy transfer from photon to electron systems near the phase transition. Our results establish the quantum phase transition as an invaluable tool for optimizing the photon-to-electron conversion in QD-cQED devices.

DOI: [10.1103/PhysRevB.108.085430](https://doi.org/10.1103/PhysRevB.108.085430)

I. INTRODUCTION

Hybrid devices, which couple quantum dots to microwave photons have received great attention due to their potential applications for controlling light-matter interactions [1–11], which has spawned a novel field of quantum-dot circuit quantum electrodynamics (QD-cQED). The QD-cQED not only provides an effective way to engineer photon statistics by tuning electron transport [12–19], but also allows one to explore photon-to-electron conversion [20–24]. With respect to the latter topic, how to control the photocurrent is one of the central goals in the QD-cQED with a significant practical relevance for quantum photovoltaics [20] and single-microwave-photon detection [21–24].

So far, much work on the photon-to-electron conversion in the QD-cQED has focused on linear microwave resonators, which can bring the unbiased QD system out of equilibrium in a controlled way, yielding inelastic electron transport. The emergence of nonlinear resonators, such as waveguides, photonic crystals, and optomechanical resonators [25–27], has been introduced to study the quantum many-body physics. The dissipative nonlinear resonators subject to a coherent or a squeezed driving field has been studied, the resultant large quantum fluctuation induced by the switching between two phases occurs, and, consequently, the first- or second-order quantum phase transitions is observed [28–32]. The realization of nonlinear QD-cQED devices is highly desirable, therefore, it is important to develop a transparent theory for revealing the effect of the nonlinearity-induced quantum fluctuations on the photon-to-electron conversion.

In this paper, we theoretically study the photon-assisted electron tunneling in a specific nonlinear QD-cQED device of a double quantum dot system capacitively coupled to a driven microwave resonator with Kerr nonlinearity. Compared to previous proposals, we focus explicitly on the consequences of the photon nonlinearity for the photocurrent with the aim to reveal the mechanism for enhancing the photon-to-electron conversion. Based on the quantum master equation, we first derive a general formula to connect photon excitation and generated photocurrent. It is found that the photon excitation exhibits a first-order quantum phase transition, which can be used to tune the electron transport process, leading to an enhancement of the photocurrent. This is attributed to the enhanced energy transfer from photon to electron systems near the phase transition.

II. MODEL

As illustrated in Fig. 1, we consider a double-quantum-dot (DQD) system interacting with a driven microwave resonator according to the Hamiltonian,

$$H(t) = H_s(t) + H_e + H_b, \quad (1)$$

$$\begin{aligned} H_s(t) = & \frac{\varepsilon_d}{2} (|L\rangle\langle L| - |R\rangle\langle R|) + t_d (|L\rangle\langle R| + |R\rangle\langle L|) \\ & + \omega_r a_r^\dagger a_r + \frac{U_r}{2} a_r^\dagger a_r^\dagger a_r a_r \\ & + 2 \cos(\omega_L t) \sqrt{\kappa_L N_L} (a_r^\dagger + a_r) \\ & + g_r (a_r^\dagger + a_r) (|L\rangle\langle L| - |R\rangle\langle R|), \end{aligned} \quad (2)$$

$$\begin{aligned} H_e = & \sum_{k,v=L,R} \varepsilon_{kv} c_{kv}^\dagger c_{kv} + \sum_k (t_{kL} c_{kL} |L\rangle\langle 0| \\ & + t_{kL}^* |0\rangle\langle L| c_{kL}^\dagger + t_{kR} c_{kR} |R\rangle\langle 0| + t_{kR}^* |0\rangle\langle R| c_{kR}^\dagger), \end{aligned} \quad (3)$$

*xiong@ynu.edu.cn

†jtl@hust.edu.cn

‡zhengbo@zju.edu.cn

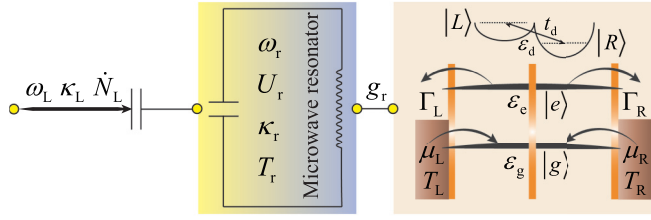


FIG. 1. Schematic of a nonlinear QD-cQED device. A microwave resonator with angular frequency ω_r and Kerr nonlinearity U_r is driven by an external laser field with frequency ω_L and incoming photon rate \dot{N}_L . The coupling between the resonator and the laser field is described by κ_L . Two quantum dots with level space ε_d and interdot tunnel rate t_d , are connected to two electrodes with chemical potential $\mu_{L,R}$ and temperature $T_{L,R}$. $\Gamma_{L,R}$ describes the coupling between the dots and the electrodes. The coupling between the electronic states $|L\rangle$ and $|R\rangle$ and the resonator is characterized by g_r , whereas, in the eigenbasis the electronic states are $|e\rangle$ and $|g\rangle$ with energies ε_e and ε_g .

$$H_b = \sum_{\alpha} \omega_{\alpha} b_{\alpha}^{\dagger} b_{\alpha} + \sum_{\alpha} (t_{\alpha r} b_{\alpha}^{\dagger} a_r + t_{\alpha r}^* b_{\alpha} a_r^{\dagger}). \quad (4)$$

Here, $H_s(t)$ is the Hamiltonian of the DQD-resonator system, which contains the isolate DQD, the driven resonator, and their coupling. ε_d is the energy space between the two electronic states $|L\rangle$ and $|R\rangle$, and t_d is the interdot tunnel coupling. The microwave resonator is modeled by a bosonic field with the creation operator a_r^{\dagger} , the angular frequency ω_r , and the Kerr nonlinearity U_r . It can be driven by a laser field with the frequency ω_L . The coupling between the resonator and the laser field is characterized by κ_L , and the rate of incident photons is \dot{N}_L . The resonator is capacitively coupled to the DQD with an energy-independent strength g_r . H_e is the Hamiltonian of the electrodes and its coupling with the electronic states in the DQD, where c_{kv}^{\dagger} is the creation operator for an electron with momentum k and energy ε_{kv} , and t_{kv} is the tunneling amplitude between the electrode v and its neighboring electron states. Finally, H_b is the Hamiltonian of the bath, and its coupling with the resonator, where b_{α}^{\dagger} is the creation operator of the photon with frequency ω_{α} , and $t_{\alpha r}$ is the bath-resonator coupling strength.

In the eigenbasis of the DQD, the ground and excited states are given by $|e\rangle = \cos(\theta/2)|L\rangle + \sin(\theta/2)|R\rangle$ and $|g\rangle = -\sin(\theta/2)|L\rangle + \cos(\theta/2)|R\rangle$ with $\theta = \arctan(2t_d/\varepsilon_d)$. Under the Born-Markov approximation, the dynamics of the DQD-resonator system in a rotating frame is governed by the following master equation [33–35]:

$$\frac{d}{dt}\rho(t) = -i[\mathcal{H}_s, \rho(t)] + \mathcal{D}_d[\rho(t)] + \mathcal{D}_r[\rho(t)], \quad (5)$$

where $\rho(t)$ is the reduced density matrix of the system and its coherent evolution is determined by the Hamiltonian,

$$\begin{aligned} \mathcal{H}_s = & \frac{\Delta_d}{2} (d_e^{\dagger} d_e - d_g^{\dagger} d_g) \\ & + \Delta_r a_r^{\dagger} a_r + \frac{U_r}{2} a_r^{\dagger} a_r^{\dagger} a_r a_r + \sqrt{\kappa_L \dot{N}_L} (a_r^{\dagger} + a_r) \\ & - g_r \sin \theta (a_r^{\dagger} d_e^{\dagger} d_e + a_r d_e^{\dagger} d_g), \end{aligned} \quad (6)$$

where $d_g^{\dagger} = |g\rangle\langle 0|$ and $d_e^{\dagger} = |e\rangle\langle 0|$ are the creation operators for the ground and excited states with the renormalized energies $\varepsilon_g = -\Omega_d/2$ and $\varepsilon_e = \Omega_d/2$, $\Omega_d = \sqrt{\varepsilon_d^2 + 4t_d^2}$ is the effective energy space. $\Delta_d = \Omega_d - \omega_L$ and $\Delta_r = \omega_r - \omega_L$ are the detunings with respect to the drive frequency. The tunneling events between the DQD and the electrodes are described by

$$\begin{aligned} \mathcal{D}_d[\rho(t)] = & \frac{1}{2} \sum_{v=L,R} \sum_{i=g,e} \Gamma_{vi}^{\theta} \{f_v(\varepsilon_i) \mathcal{D}[d_i^{\dagger}, \rho(t)] \\ & + (1 - f_v(\varepsilon_i)) \mathcal{D}[d_i, \rho(t)]\}, \end{aligned} \quad (7)$$

and the resonator-bath energy exchange is described by

$$\begin{aligned} \mathcal{D}_r[\rho(t)] = & \frac{\kappa_r}{2} \{n_B(\omega_r) \mathcal{D}[a_r^{\dagger}, \rho(t)] \\ & + [1 + n_B(\omega_r)] \mathcal{D}[a_r, \rho(t)]\}, \end{aligned} \quad (8)$$

where the superoperators act according to $\mathcal{D}[O, \rho(t)] = 2O\rho(t)O^{\dagger} - O^{\dagger}O\rho(t) - \rho(t)O^{\dagger}O$ for the arbitrary operator O . The electronic states in electrode v are occupied according to the Fermi-Dirac distribution $f_v(\varepsilon_i) = \{\exp[(\varepsilon_i - \mu_v)/k_B T_v] + 1\}^{-1}$ with chemical potential μ_v and temperature T_v . The tunneling rates of electrons are characterized by Γ_{vi}^{θ} with $\Gamma_{Le}^{\theta} = \Gamma_L \cos^2(\theta/2)$, $\Gamma_{Rg}^{\theta} = \Gamma_R \cos^2(\theta/2)$, $\Gamma_{Lg}^{\theta} = \Gamma_L \sin^2(\theta/2)$, and $\Gamma_{Re}^{\theta} = \Gamma_R \sin^2(\theta/2)$, where $\Gamma_v(\varepsilon) = 2\pi \sum_k |t_{kv}|^2 \delta(\varepsilon - \varepsilon_{kv})$. The average occupation of the resonator in equilibrium state at temperature T_r is described by the Bose-Einstein distribution $n_B(\omega_r) = [\exp(\hbar\omega_r/k_B T_r) - 1]^{-1}$. $\kappa_r(\omega) = 2\pi \sum_{\alpha} |t_{\alpha r}|^2 \delta(\omega - \omega_{\alpha})$ is the dissipation rate of the resonator. Here, we assume that $\Gamma_v(\varepsilon)$ and $\kappa_r(\omega)$ are independent of energy and frequency.

Without the electron-photon coupling for $g_r = 0$, upon adjusting the driven strength the steady state of the nonlinear resonator system may undergo a sudden jump, which is manifested in a discontinuity in the photon density of the resonator. It realizes a dissipative quantum phase transition in nonequilibrium steady states [28–30, 36–40]. When we consider extended systems as described by the nonlinear QD-cQED in Fig. 1 with $g_r \neq 0$, such nonlinear resonator systems can unlock their potential in the photon-assisted electron transport. The photon jumps are, thus, expected to regulate the photocurrent flowing through the DQD system.

III. RELATION OF PHOTON EXCITATION AND ELECTRON TRANSPORT

We are interested in the electron transport excited by the driven resonator. For $\mu_L = \mu_R = 0$ and $T_v = T_r = 0$, an electron can be injected from one electrode to level g , it can tunnel to level e by absorbing a photon from the driven resonator and then tunnel to another electrode. Hence, the electron transport and, thus, the electrical current in the DQD system can be generated, which is similar to the conventional photon-assisted tunneling where the electrons are coupled to the electromagnetic fields with classical or quantum

description [20,24,41,42]. The time evolution of the average value of the DQD and photon operators are given by

$$\frac{d}{dt}\langle N_Q \rangle = (\Gamma_{Lg}^\theta + \Gamma_{Rg}^\theta)\langle \sigma_0 \rangle - (\Gamma_{Le}^\theta + \Gamma_{Re}^\theta)\langle \sigma_e \rangle, \quad (9)$$

$$\begin{aligned} \frac{d}{dt}\langle \sigma_z \rangle = & -i[2g_r \sin \theta (\langle a_r^\dagger d_g^\dagger d_e \rangle - \langle a_r d_e^\dagger d_g \rangle)] \\ & - (\Gamma_{Lg}^\theta + \Gamma_{Rg}^\theta)\langle \sigma_0 \rangle - (\Gamma_{Le}^\theta + \Gamma_{Re}^\theta)\langle \sigma_e \rangle, \end{aligned} \quad (10)$$

$$\begin{aligned} \frac{d}{dt}\langle a_r^\dagger a_r \rangle = & -i[\sqrt{\kappa_L \dot{N}_L}(\langle a_r^\dagger \rangle - \langle a_r \rangle) \\ & - g_r \sin \theta (\langle a_r^\dagger d_g^\dagger d_e \rangle - \langle a_r d_e^\dagger d_g \rangle)] - \kappa_r \langle a_r^\dagger a_r \rangle, \end{aligned} \quad (11)$$

where $N_Q = |e\rangle\langle e| + |g\rangle\langle g|$, $\sigma_z = |e\rangle\langle e| - |g\rangle\langle g|$, $\sigma_e = |e\rangle\langle e|$, and $\sigma_0 = |0\rangle\langle 0|$ with the constraint $|0\rangle\langle 0| + |g\rangle\langle g| + |e\rangle\langle e| = 1$. The expectation value of a system operator is calculated by $\langle O \rangle = \text{Tr}\{O\rho(t)\}$. The rate of change in the DQD population determines the particle current,

$$\frac{d}{dt}\langle N_Q \rangle = I_L(t) - I_R(t), \quad (12)$$

where $I_L(t)$ and $-I_R(t)$ are the currents from left and right electrodes, and Eq. (9) gives

$$I_L(t) = \Gamma_{Lg}^\theta \langle \sigma_0 \rangle - \Gamma_{Le}^\theta \langle \sigma_e \rangle, \quad (13)$$

$$I_R(t) = -(\Gamma_{Rg}^\theta \langle \sigma_0 \rangle - \Gamma_{Re}^\theta \langle \sigma_e \rangle). \quad (14)$$

In the steady state for $t \rightarrow \infty$, the photocurrent can be defined as $I_{pe} := -eI_R$, which is given by Eqs. (9)–(11),

$$\begin{aligned} I_{pe} = & e \left(\frac{\Gamma_{Re}^\theta}{\Gamma_{Le}^\theta + \Gamma_{Re}^\theta} - \frac{\Gamma_{Rg}^\theta}{\Gamma_{Lg}^\theta + \Gamma_{Rg}^\theta} \right) \\ & \times (\sqrt{2\kappa_L \dot{N}_L} \langle p_r \rangle + \kappa_r \langle a_r^\dagger a_r \rangle), \end{aligned} \quad (15)$$

where $p_r = i(a_r^\dagger - a_r)/\sqrt{2}$ is the momentum operator of the resonator. $I_{pe} > 0$ indicates the electron transport from right to left, whereas, $I_{pe} < 0$ corresponds to the opposite process. To this extent, the relation between the photocurrent and the photon excitation is established.

IV. ENHANCING PHOTOCURRENT BY QUANTUM PHASE TRANSITION

Obviously, Eq. (15) describes the contribution to I_{pe} due to the joint DQD-electrode coupling ratio $\Gamma_c = \Gamma_{Re}^\theta/(\Gamma_{Le}^\theta + \Gamma_{Re}^\theta) - \Gamma_{Rg}^\theta/(\Gamma_{Lg}^\theta + \Gamma_{Rg}^\theta)$ and the photon excitation $N_{re} = \sqrt{\kappa_L \dot{N}_L} \langle p_r \rangle + \kappa_r \langle a_r^\dagger a_r \rangle$, respectively. For a given θ , $\Gamma_L \gg \Gamma_R$ or $\Gamma_L \ll \Gamma_R$ will significantly reduce Γ_c and, thus, I_{pe} . To optimize the photocurrent, we consider symmetric DQD-electrode couplings and take $\Gamma_L = \Gamma_R = \Gamma_0$ thereby $\Gamma_c = -\cos \theta$ and $I_{pe} = -e \cos \theta N_{re}$. Moreover, when $\theta = 0$ induced by $t_d = 0$, the photocurrent vanishes due to $N_{re} = 0$ as indicated by Eq. (11). A further inspection of Eq. (15) reveals that, under the external coherent driven, the excited resonator dominates the photocurrent. It is possible to optimize the photon-to-electron conversion by engineering the resonator.

Here, we focus on how to control the photon-to-electron conversion by Kerr nonlinearity, and its effect on the

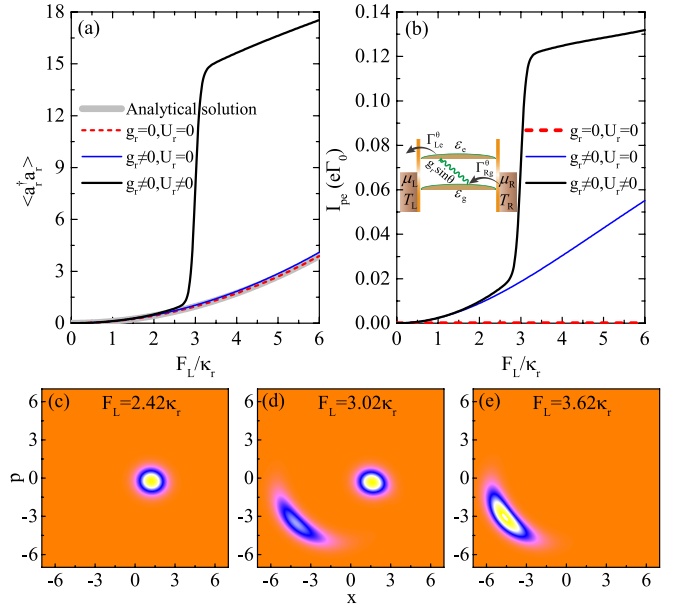


FIG. 2. (a) Mean photon number $\langle a_r^\dagger a_r \rangle$ as a function of the drive strength $F_L = \sqrt{\kappa_L \dot{N}_L}$. The analytical solution is calculated by Eqs. (11) and (16). (b) Similar to (a), but for the photocurrent versus F_L . The inset in (b) shows the transport process in the eigenbasis. (c) Wigner functions for $F_L = 2.42\kappa_r$, $F_L = 3.02\kappa_r$, and $F_L = 3.62\kappa_r$. The other parameters are $\varepsilon_d = 4.84$ GHz, $t_d = 3.96$ GHz, $\kappa_r = 0.025$ GHz, $\omega_r = \Omega_d$, $g_r = 0.7\kappa_r$, $\omega_L = \Omega_d + 3\kappa_r$, $U_r = 0.25\kappa_r$, and $\Gamma_0 = 0.8\kappa_r$.

photocurrent is encoded in the resonator momentum,

$$\langle p_r \rangle = \sqrt{2} \text{Im} \left[\frac{U_r \langle a_r^\dagger a_r^\dagger a_r \rangle + \sqrt{\kappa_L \dot{N}_L} - g_r \sin \theta \langle d_e^\dagger d_g \rangle}{\Delta_r + \frac{i\kappa_r}{2}} \right], \quad (16)$$

where we first investigate the case for $U_r = 0$ and $g_r = 0$, then $\langle p_r \rangle = -\kappa_r \sqrt{\kappa_L \dot{N}_L} / [\sqrt{2}(\Delta_r^2 + \frac{\kappa_r^2}{4})]$, $\langle a_r^\dagger a_r \rangle = \kappa_L \dot{N}_L / (\Delta_r^2 + \frac{\kappa_r^2}{4})$, and $I_{pe} = 0$. As shown in Fig. 2(a), a trivial excitation dominated by the laser field with $\langle a_r^\dagger a_r \rangle \propto F_L^2$ can be achieved, which is consistent with the numerical solution. For $g_r \neq 0$ and $U_r = 0$, our model recovers the conventional photon-to-electron configuration where the relation of $\langle a_r^\dagger a_r \rangle \propto F_L^2$ is almost not affected by the electron-photon interaction, and a similar behavior also holds in the photocurrent in Fig. 2(b). However, for $g_r \neq 0$ and $U_r \neq 0$, we access a discontinuous jump in $\langle a_r^\dagger a_r \rangle$ and may, hence, enhance the photocurrent I_{pe} . Note that, $I_{pe} > 0$ means the electrons move from right to left, resulting from the processes with $\tan^2(\theta/2) < 1$ in the inset of Fig. 2(b).

The discontinuous jump relevant to our model is critical in revealing the occurrence of the nonlinearity-enhanced photocurrent. Although the changes in $\langle a_r^\dagger a_r \rangle$ can capture the discontinuous jump, whereas, the mechanism cannot be assessed by simply measuring $\langle a_r^\dagger a_r \rangle$. Thus, we introduce the Wigner function [43,44], defined by $W(x, p) = \frac{1}{\pi} \int \langle x + \xi | \rho | x - \xi \rangle e^{-2ip\xi} d\xi$ to reveal such a excitation mechanism of the resonator. The Wigner distributions in Figs. 2(c)–2(e) are shown before, near, and after the discontinuous jump,

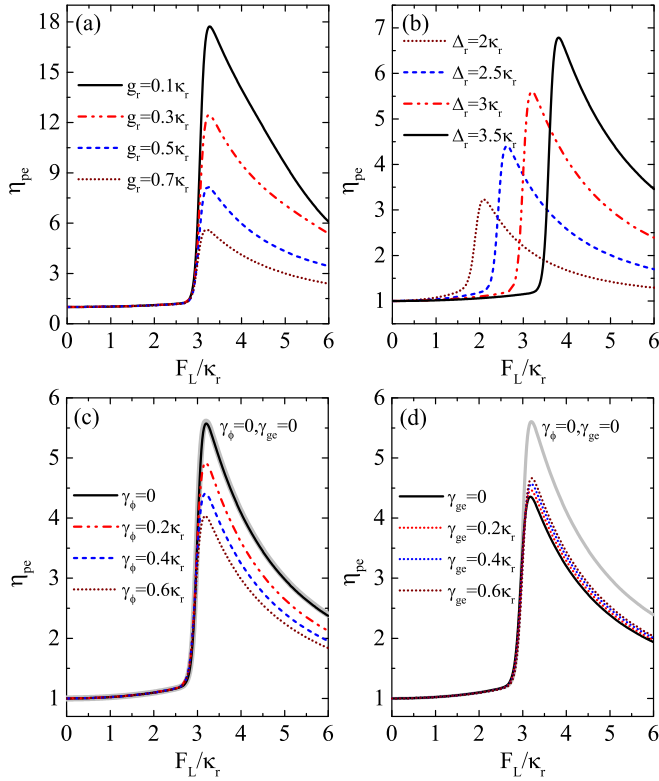


FIG. 3. (a) Performance of photon-to-electron conversion η_{pe} as a function of the drive strength F_L for indicated values of the electron-photon strength g_r . (b) Similar to (a), but for η_{pe} versus F_L for indicated values of the detuning Δ_r with $\Delta_d = \Delta_r$. (c) Similar to (a), but for η_{pe} versus F_L for indicated values of the electronic dephasing γ_ϕ with $\gamma_{ge} = 0.05\kappa_r$. (d) Similar to (a), but for η_{pe} versus F_L for indicated values of the electronic relaxation γ_{ge} with $\gamma_\phi = 0.2\kappa_r$. The other parameters are the same as in Fig. 2.

respectively. Before and after the discontinuous jump, the Wigner distribution shows a transition between two regions in phase space. Near the discontinuous jump, two peaks in the Wigner distribution develop as a consequence of the optical bistability. This qualitatively confirms the presence of the first-order quantum phase transition, similar to that observed in a laser-driven Kerr cavity [28–30,38–40]. We can, therefore, attribute the enhanced photocurrent to the nonlinearity-induced first-order quantum phase transition. To be specific, $\langle a_r^\dagger a_r \rangle$ and $\langle p_r \rangle$ undergo such a phase transition by tuning F_L , and the joint effect indicated by Eq. (15) allows the transition of I_{pe} thereby enabling the enhancement of the photon-to-electron conversion.

To characterize the ability of the phase transition to adjust the photocurrent, the performance can be quantified by the ratio between the electron transport with U_r and the one without U_r ,

$$\eta_{pe} = \frac{I_{pe}(U_r \neq 0)}{I_{pe}(U_r = 0)}, \quad (17)$$

as displayed in Fig. 3(a). Varying g_r does not shift the phase transition point at $F_L \approx 3\kappa_r$, where $\eta_{pe} > 1$ is achieved. When g_r is increased, we observe a decrease in η_{pe} around the phase transition. This can be revealed by another expression

for the photocurrent $I_{pe} = ie\Gamma_c g_r \sin \theta (\langle a_r^\dagger d_g^\dagger d_e \rangle - \langle a_r d_e^\dagger d_g \rangle)$, indicating that I_{pe} increases to some extent with increasing g_r for both $U_r = 0$ and $U_r \neq 0$. Figure 3(b) shows η_{pe} versus F_L for different Δ_r 's. The value of η_{pe} around the phase transition significantly increases with Δ_r , and the maximum position is shifted toward large values of F_L . This is because the phase transition point can be adjusted by Δ_r as indicated by Eqs. (11) and (16). We further discuss how the performance I_{pe} is affected by the electronic dephasing and relaxation, which can be characterized by $\mathcal{D}_\phi[\rho(t)] = (\gamma_\phi/2)[\sigma_z, \rho(t)]$ and $\mathcal{D}_{ge}[\rho(t)] = (\gamma_{ge}/2)[d_g^\dagger d_e, \rho(t)]$ with the rates γ_ϕ and γ_{ge} . By adding $\mathcal{D}_\phi[\rho(t)]$ and $\mathcal{D}_{ge}[\rho(t)]$ into Eq. (5), we find that the enhanced photocurrent near phase transition is robust with respect to the electronic dephasing and relaxation as shown in Figs. 3(c) and 3(d).

V. ENERGY TRANSPORT

The DQD and the laser-driven resonator only exchange energy rather than the electron. Thus, the mechanism of the phase-transition enhanced photocurrent can be revealed in the energy transport process where the energy flux through the DQD is given by [45]

$$\dot{E}_d = \text{Tr} \left\{ \frac{d\rho(t)}{dt} \mathcal{H}_d \right\} =: J_{pe}(t) + J_L(t) + J_R(t), \quad (18)$$

where $\mathcal{H}_d = \Delta_d(d_e^\dagger d_e - d_g^\dagger d_g)/2$. $J_{pe}(t)$ is the DQD-resonator interaction energy and can be expressed as

$$J_{pe}(t) = ig_r \sin \theta \Delta_d \text{Tr} \{ (a_r d_e^\dagger d_g - a_r^\dagger d_g^\dagger d_e) \rho(t) \}, \quad (19)$$

whereas, $J_{L,R}(t)$ is the DQD-electrode exchange energy,

$$J_v(t) = -\frac{\Delta_d}{2} \text{Tr} \{ (\Gamma_{vg}^\theta \sigma_0 + \Gamma_{ve}^\theta \sigma_e) \rho(t) \}, \quad v = L, R. \quad (20)$$

For $g_r = 0$, the resonator is disconnected from the unbiased DQD, such that the DQD-resonator energy exchange vanishes. For $g_r \neq 0$, connecting the resonator to the DQD allows DQD-resonator energy exchange to occur. From Eq. (11), $J_{pe}(t)$ can be rewritten as $J_{pe} = \Delta_d(\sqrt{2\kappa_L \bar{N}} \langle p_r \rangle + \kappa_r \langle a_r^\dagger a_r \rangle)$ in the steady state for $t \rightarrow \infty$. We observe that the resonator excitation $\langle p_r \rangle$ and $\langle a_r^\dagger a_r \rangle$ in J_{pe} , which are similar to that described for I_{pe} , have the effect of engineering energy transport. In Fig. 4, we plot J_{pe} and $J_e (= J_L + J_R)$ versus F_L with $g_r \neq 0$ for $U_r = 0$ and $U_r \neq 0$. For $U_r = 0$, a trivial energy transport with $J_{pe} \propto F_L^2$ is observed. However, for $U_r \neq 0$, J_{pe} is increased in the vicinity of the additional transition, and $J_{pe}(U_r \neq 0)/J_{pe}(U_r = 0)$ in the inset can highlight such an enhancement. We can interpret this phenomenon as the phase-transition enhanced energy transport. Note that, the first law of thermodynamics, indicated by $J_{pe} + J_e = 0$, always holds for both $U_r = 0$ and $U_r \neq 0$. Clearly, the phase transition induced by resonator engineering can be used to enhance the energy transfer from photon to electron systems, thus, achieving an enhancement of the photon-to-electron conversion.

Our results rely on the Kerr-like nonlinearity of the resonator, which is of immediate relevance to real physical systems, such as Fabry-Pérot microcavities filled by nonlinear medium [46], semiconductor microcavities [29,38], on-chip

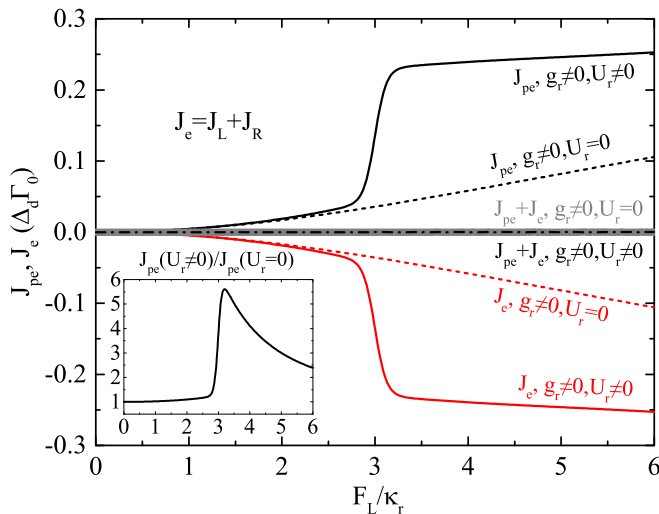


FIG. 4. Energy fluxes J_{pe} and J_e as a function of the drive strength F_L for different values of g_r and U_r . The inset shows $J_{pe}(U_r \neq 0)/J_{pe}(U_r = 0)$. The other parameters are the same as in Fig. 2.

superconducting nonlinear resonators [47], and quantum circuits [48,49]. The driven-dissipative Kerr models for studying the out-of-equilibrium critical behaviors have been

realized experimentally [29,30,38,50]. When such systems are capacitively coupled to a QD system [3,23,51], the nonlinear QD-cQED devices and, thus, the photon-assisted electron transport becomes possible, enabling highlight the nonlinear effects.

VI. CONCLUSIONS

We propose a nonlinear QD-cQED setup consisting of a double quantum dot system and a nonlinear microwave resonator and reveal that the photon excitation undergoes a first-order quantum phase transition, and it can be used to tune the inelastic electron transport in quantum dots. The photocurrent is enhanced around the phase transition since the energy transfer from photon to electron systems is increased. Our results pave the way to control photon-to-electron conversion by the quantum phase transition in QD-cQED devices.

ACKNOWLEDGMENTS

The work was supported by the National Natural Science Foundation of China (Grants No. 12204405, No. 12105242, No. 21873033, No. 22273029, No. 12175193, and No. 11775186) and by the Yunnan Fundamental Research Project (Grants No. 202301AT070108, No. 202201AT070161, and No. 202301AW070006).

- [1] J. Viennot, M. Dartiailh, A. Cottet, and T. Kontos, Coherent coupling of a single spin to microwave cavity photons, *Science* **349**, 408 (2015).
- [2] G.-W. Deng, D. Wei, S.-X. Li, J. Johansson, W.-C. Kong, H.-O. Li, G. Cao, M. Xiao, G.-C. Guo *et al.*, Coupling two distant double quantum dots with a microwave resonator, *Nano Lett.* **15**, 6620 (2015).
- [3] X. Mi, J. Cady, D. Zajac, P. Deelman, and J. R. Petta, Strong coupling of a single electron in silicon to a microwave photon, *Science* **355**, 156 (2017).
- [4] A. Stockklauser, P. Scarlino, J. V. Koski, S. Gasparinetti, C. K. Andersen, C. Reichl, W. Wegscheider, T. Ihn, K. Ensslin, and A. Wallraff, Strong Coupling Cavity QED with Gate-Defined Double Quantum Dots Enabled by a High Impedance Resonator, *Phys. Rev. X* **7**, 011030 (2017).
- [5] A. J. Landig, J. V. Koski, P. Scarlino, U. Mendes, A. Blais, C. Reichl, W. Wegscheider, A. Wallraff, K. Ensslin, and T. Ihn, Coherent spin-photon coupling using a resonant exchange qubit, *Nature (London)* **560**, 179 (2018).
- [6] N. Samkharadze, G. Zheng, N. Kalhor, D. Brousse, A. Sammak, U. Mendes, A. Blais, G. Scappucci, and L. Vandersypen, Strong spin-photon coupling in silicon, *Science* **359**, 1123 (2018).
- [7] X. Mi, M. Benito, S. Putz, D. M. Zajac, J. M. Taylor, G. Burkard, and J. R. Petta, A coherent spin-photon interface in silicon, *Nature (London)* **555**, 599 (2018).
- [8] F. Borjans, X. Croot, X. Mi, M. Gullans, and J. Petta, Resonant microwave-mediated interactions between distant electron spins, *Nature (London)* **577**, 195 (2020).
- [9] A. Purkayastha, M. Kulkarni, and Y. N. Joglekar, Emergent PT symmetry in a double-quantum-dot circuit QED setup, *Phys. Rev. Res.* **2**, 043075 (2020).
- [10] F. Hellbach, F. Pauly, W. Belzig, and G. Rastelli, Quantum-correlated photons generated by nonlocal electron transport, *Phys. Rev. B* **105**, L241407 (2022).
- [11] S. Haldar, H. Havir, W. Khan, S. Lehmann, C. Thelander, K. A. Dick, and V. F. Maisi, Energetics of Microwaves Probed by Double Quantum Dot Absorption, *Phys. Rev. Lett.* **130**, 087003 (2023).
- [12] C. Xu and M. G. Vavilov, Full counting statistics of photons emitted by a double quantum dot, *Phys. Rev. B* **88**, 195307 (2013).
- [13] M. Kulkarni, O. Cotlet, and H. E. Türeci, Cavity-coupled double-quantum dot at finite bias: Analogy with lasers and beyond, *Phys. Rev. B* **90**, 125402 (2014).
- [14] M. Marthaler, Y. Utsumi, and D. S. Golubev, Lasing in circuit quantum electrodynamics with strong noise, *Phys. Rev. B* **91**, 184515 (2015).
- [15] N. Lambert, F. Nori, and C. Flindt, Bistable Photon Emission from a Solid-State Single-Atom Laser, *Phys. Rev. Lett.* **115**, 216803 (2015).
- [16] G. Rastelli and M. Governale, Single atom laser in normal-superconductor quantum dots, *Phys. Rev. B* **100**, 085435 (2019).
- [17] B. K. Agarwalla, M. Kulkarni, and D. Segal, Photon statistics of a double quantum dot micromaser: Quantum treatment, *Phys. Rev. B* **100**, 035412 (2019).
- [18] M. Mantovani, A. D. Armour, W. Belzig, and G. Rastelli, Dynamical multistability in a quantum-dot laser, *Phys. Rev. B* **99**, 045442 (2019).
- [19] L.-L. Nian, B. Zheng, and J.-T. Lü, Electrically driven photon statistics engineering in quantum-dot circuit quantum electrodynamics, *Phys. Rev. B* **107**, L241405 (2023).

- [20] C. Xu and M. G. Vavilov, Quantum photovoltaic effect in double quantum dots, *Phys. Rev. B* **87**, 035429 (2013).
- [21] C. H. Wong and M. G. Vavilov, Quantum efficiency of a single microwave photon detector based on a semiconductor double quantum dot, *Phys. Rev. A* **95**, 012325 (2017).
- [22] A. Ghirri, S. Cornia, and M. Affronte, Microwave photon detectors based on semiconducting double quantum dots, *Sensors* **20**, 4010 (2020).
- [23] W. Khan, P. P. Potts, S. Lehmann, C. Thelander, K. A. Dick, P. Samuelsson, and V. F. Maisi, Efficient and continuous microwave photoconversion in hybrid cavity-semiconductor nanowire double quantum dot diodes, *Nat. Commun.* **12**, 5130 (2021).
- [24] D. Zenelaj, P. P. Potts, and P. Samuelsson, Full counting statistics of the photocurrent through a double quantum dot embedded in a driven microwave resonator, *Phys. Rev. B* **106**, 205135 (2022).
- [25] J. W. Fleischer, M. Segev, N. K. Efremidis, and D. N. Christodoulides, Observation of two-dimensional discrete solitons in optically induced nonlinear photonic lattices, *Nature (London)* **422**, 147 (2003).
- [26] M. Eichenfield, J. Chan, R. M. Camacho, K. J. Vahala, and O. Painter, Optomechanical crystals, *Nature (London)* **462**, 78 (2009).
- [27] P. Hamel, S. Haddadi, F. Raineri, P. Monnier, G. Beaudoin, I. Sagnes, A. Levenson, and A. M. Yacomotti, Spontaneous mirror-symmetry breaking in coupled photonic-crystal nanolasers, *Nat. Photon.* **9**, 311 (2015).
- [28] W. Casteels, R. Fazio, and C. Ciuti, Critical dynamical properties of a first-order dissipative phase transition, *Phys. Rev. A* **95**, 012128 (2017).
- [29] S. R. K. Rodriguez, W. Casteels, F. Storme, N. Carlon Zambon, I. Sagnes, L. Le Gratiet, E. Galopin, A. Lemaître, A. Amo, C. Ciuti, and J. Bloch, Probing a Dissipative Phase Transition via Dynamical Optical Hysteresis, *Phys. Rev. Lett.* **118**, 247402 (2017).
- [30] P. Brookes, G. Tancredi, A. D. Patterson, J. Rahamim, M. Esposito, T. K. Mavrogordatos, P. J. Leek, E. Ginossar, and M. H. Szymanska, Critical slowing down in circuit quantum electrodynamics, *Sci. Adv.* **7**, eabe9492 (2021).
- [31] W. Casteels and C. Ciuti, Quantum entanglement in the spatial-symmetry-breaking phase transition of a driven-dissipative bose-hubbard dimer, *Phys. Rev. A* **95**, 013812 (2017).
- [32] X. H. H. Zhang and H. U. Baranger, Driven-dissipative phase transition in a kerr oscillator: From semiclassical pt symmetry to quantum fluctuations, *Phys. Rev. A* **103**, 033711 (2021).
- [33] G. Lindblad, On the generators of quantum dynamical semi-groups, *Commun. Math. Phys.* **48**, 119 (1976).
- [34] H.-P. Breuer and F. Petruccione, *The Theory of Open Quantum Systems* (Oxford University Press, Oxford, 2002).
- [35] H. J. Carmichael, *Statistical Methods in Quantum Optics I: Master Equations and Fokker-Planck Equations* (Springer, Berlin, 2013).
- [36] P. Drummond and D. Walls, Quantum theory of optical bistability. I. Nonlinear polarisability model, *J. Phys. A* **13**, 725 (1980).
- [37] M. A. Macovei, Measuring photon-photon interactions via photon detection, *Phys. Rev. A* **82**, 063815 (2010).
- [38] T. Fink, A. Schade, S. Höfling, C. Schneider, and A. Imamoglu, Signatures of a dissipative phase transition in photon correlation measurements, *Nat. Phys.* **14**, 365 (2018).
- [39] F. Minganti, A. Biella, N. Bartolo, and C. Ciuti, Spectral theory of liouvillians for dissipative phase transitions, *Phys. Rev. A* **98**, 042118 (2018).
- [40] B. O. Goes and G. T. Landi, Entropy production dynamics in quench protocols of a driven-dissipative critical system, *Phys. Rev. A* **102**, 052202 (2020).
- [41] T. H. Stoof and Yu. V. Nazarov, Time-dependent resonant tunneling via two discrete states, *Phys. Rev. B* **53**, 1050 (1996).
- [42] M. H. Pedersen and M. Büttiker, Scattering theory of photon-assisted electron transport, *Phys. Rev. B* **58**, 12993 (1998).
- [43] J. R. Johansson, P. D. Nation, and F. Nori, QuTiP: An open-source python framework for the dynamics of open quantum systems, *Comput. Phys. Commun.* **183**, 1760 (2012).
- [44] J. R. Johansson, P. D. Nation, and F. Nori, QuTiP 2: An open-source python framework for the dynamics of open quantum systems, *Comput. Phys. Commun.* **184**, 1234 (2013).
- [45] E. Boukobza and D. J. Tannor, Thermodynamics of bipartite systems: Application to light-matter interactions, *Phys. Rev. A* **74**, 063823 (2006).
- [46] H. Gibbs, S. McCall, and T. Venkatesan, Differential Gain and Bistability Using a Sodium-Filled Fabry-Perot Interferometer, *Phys. Rev. Lett.* **36**, 1135 (1976).
- [47] Z. Wang, M. Pechal, E. A. Wollack, P. Arrangoiz-Arriola, M. Gao, N. R. Lee, and A. H. Safavi-Naeini, Quantum Dynamics of a Few-Photon Parametric Oscillator, *Phys. Rev. X* **9**, 021049 (2019).
- [48] S. Rebić, J. Twamley, and G. J. Milburn, Giant Kerr Nonlinearities in Circuit Quantum Electrodynamics, *Phys. Rev. Lett.* **103**, 150503 (2009).
- [49] A. Blais, A. L. Grimsmo, S. M. Girvin, and A. Wallraff, Circuit quantum electrodynamics, *Rev. Mod. Phys.* **93**, 025005 (2021).
- [50] Z. Geng, K. J. H. Peters, A. A. P. Trichet, K. Malmir, R. Kolkowski, J. M. Smith, and S. R. K. Rodriguez, Universal Scaling in the Dynamic Hysteresis, and Non-Markovian Dynamics, of a Tunable Optical Cavity, *Phys. Rev. Lett.* **124**, 153603 (2020).
- [51] A. Stockklauser, V. F. Maisi, J. Basset, K. Cujia, C. Reichl, W. Wegscheider, T. Ihn, A. Wallraff, and K. Ensslin, Microwave Emission from Hybridized States in a Semiconductor Charge Qubit, *Phys. Rev. Lett.* **115**, 046802 (2015).